

Zero-shot segmentation of skin tumors in whole-slide images with vision-language foundation models

Santiago Moreno*¹, Pablo Meseguer*¹, Rocío del Amor^{1,2}, Valery Naranjo^{1,2}

¹ Instituto Universitario de Investigación en Tecnología Centrada en el Ser Humano (HUMAN-Tech),

Universitat Politècnica de Valencia, Valencia, Spain

² Artikode Intelligence S.L., Valencia, Spain

{smorpin, pabmees, madeam2, vnaranjo}@upv.es

*Contributed equally

Abstract

Accurate annotation of cutaneous neoplasm biopsies represents a major challenge due to their wide morphological variability, overlapping histological patterns, and the subtle distinctions between benign and malignant lesions. Vision-language foundation models (VLMs), pre-trained on paired image-text corpora, learn joint representations that bridge visual features and diagnostic terminology, enabling zero-shot localization and classification of tissue regions without pixel-level labels. However, most existing VLM applications in histopathology remain limited to slide-level tasks or rely on coarse interactive prompts, and they struggle to produce fine-grained segmentations across gigapixel whole-slide images (WSIs). In this work, we introduce a Zero-shot visual-language segmentation pipeline for whole-slide images (ZEUS), a fully automated, zero-shot segmentation framework that leverages class-specific textual prompt ensembles and frozen VLM encoders to generate high-resolution tumor masks in WSIs. By partitioning each WSI into overlapping patches, extracting visual embeddings, and computing cosine similarities against text prompts in order to generate a final segmentation mask. We demonstrate competitive performance on two in-house datasets, primary spindle cell neoplasms and cutaneous metastases, highlighting the influence of prompt design, domain shifts, and institutional variability in VLMs for histopathology. ZEUS markedly reduces annotation burden while offering scalable, explainable tumor delineation for downstream diagnostic workflows.

1 Introduction

Skin cancer ranks among the most common malignancies globally, with incidence rates continuing to raise [1]. Cutaneous spindle-cell (CSC) neoplasms form a heterogeneous group of skin tumors, including benign leiomyomas and aggressive leiomyosarcomas, which frequently confuse pathologists due to their morphological overlap [2]. Cutaneous metastases (CM), often originating from breast or other organs, introduce additional diagnostic complexity, particularly when tracing the primary source of lesions [3].

Deep learning has revolutionized computational pathology (CPath), showing promising results in tumor detection and region-of-interest (ROI) segmentation [4, 5]. This accurate segmentation is crucial, as it helps identify ROIs and differentiate between tumor and healthy cells, thus improving

diagnostic accuracy and downstream quantitative analysis [4]. However, training such models is often hindered by the scarcity of labeled data and the labor-intensive process of manual pixel-level annotation, which remains a critical bottleneck in the development of robust, generalizable systems [5].

Foundation models, which are large-scale general-purpose AI systems trained across diverse data modalities, have recently emerged as powerful tools in CPath. These models support a wide range of downstream applications, such as rare disease classification, survival prediction, multi-stain analysis, and biomarker assessment [6]. In particular, vision-language models (VLMs) enable zero-shot classification and segmentation by linking histological imaging with associated textual data, enabling them to generalize to new tasks and reducing the reliance on exhaustive pixel-level annotations [7, 8]. While their performance in classification and retrieval tasks has been explored, their potential for zero-shot segmentation in complex biomedical scenarios remains under-investigated.

Recent studies have explored zero-shot applications of the Segment Anything Model (SAM) across diverse medical imaging modalities demonstrating its flexibility but also its dependence on user-provided prompts for accurate region delineation [9, 10]. Despite these advances, accurately segmenting diagnostically relevant regions within gigapixel WSIs remains a major hurdle, especially given that CSC and CM lesions often exhibit ambiguous pathological features. In this work, we propose Zero-shot visual-language segmentation pipeline for whole-slide images (ZEUS) that automatically generates accurate segmentations without requiring any task-specific annotations, thus automating the segmentation of tumor regions in gigapixel WSIs and significantly reducing the laborious pixel-level annotation burden on pathologists. Code for using this framework is available at <https://github.com/cvblab/ZEUS>.

2 Methodology

Figure 1 illustrates our ZEUS workflow for zero-shot ROI segmentation in gigapixel WSIs. Below, we formalize the

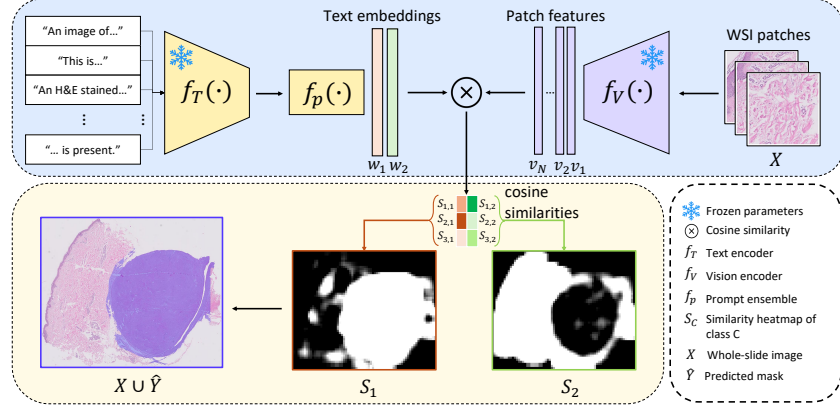


Figure 1. Overview of ZEUS workflow. **Top:** a pre-trained vision encoder (f_V) is used to extract features from WSI patches (v_N). Textual prompts for the C classes are encoded using the text encoder (f_T) to obtain the text embeddings and the ensembling function (f_p) to obtain the prompt ensembles. **Bottom:** Cosine similarities ($s_{j,c}$) between text and patch embeddings yield class-specific similarity maps (S_C), which are stacked and passed through a pixel-wise arg max to generate the final segmentation mask \hat{Y} .

problem and detail each pipeline component.

Problem formulation: WSIs are gigapixel-scale images of tissue sections (X), making direct pixel-level processing infeasible. Our goal is to automatically segment tumor versus healthy regions in these images without any pixel-level annotations. To this end, each WSI is first divided into K patches (tiles), such as $X = \{x_j\}_{j=1}^K$, from which feature embeddings are extracted using a pre-trained vision encoder (f_V). Simultaneously, we define a prompt ensemble for each class. For each tile, we compute cosine similarities against all class embeddings in order to obtain the prediction masks.

2.1 Zero-Shot Segmentation

Text encoding (Prompt ensembling): For each class c , we first assemble a set of N classnames $\{\text{classname}_n^c\}_{n=1}^N$ and a shared set of M textual templates $\{\tau_m\}_{m=1}^M$ (e.g., “an image of *CLASSNAME*,” “microscopic view of *CLASSNAME* cells”), each containing a placeholder for the classname. We then generate a prompt ensemble by substituting every classname into every template, producing $N \times M$ prompts. Specifically:

$$p_{n,m}^c = \tau_m(\text{classname}_n^c).$$

Each prompt is encoded through the VLM text encoder $f_T(\cdot)$, and all embeddings are averaged to form a single text embedding vector:

$$w_c = \frac{1}{NM} \sum_{n=1}^N \sum_{m=1}^M f_T(p_{n,m}^c). \quad (1)$$

This prompt-ensembling strategy captures diverse textual descriptions for each class and yields robust zero-shot prototypes [11, 12].

Vision encoding: Histopathology VLMs employ a vision encoder f_V (e.g., a ViT backbone) pretrained on large collections of WSIs. For each input WSI, we first partition the tissue region into K patches. Each patch x_j is then passed

through the vision encoder to obtain a D -dimensional feature vector:

$$v_j = f_V(x_j) \quad (2)$$

These patch-level embeddings $\{v_j\}_{j=1}^K$ capture local morphological and textural features, forming the visual basis for downstream ROI identification and multimodal alignment.

Multimodal alignment: Given the set of patch embeddings and the C class ensembles obtained via Eq. 1, we compute a similarity score for each patch–class pair via cosine similarity:

$$s_{j,c} = \frac{v_j \cdot w_c}{\|v_j\| \|w_c\|}, \quad (3)$$

Next, we reconstruct C per-class similarity maps $\{S_c\}_{c=1}^C$ over the original WSI by assigning each patch’s score to all of its constituent pixels. When the patching process involves overlap, we calculate the average similarity across the overlapping pixels. Formally, if pixel p belongs to tile j , then

$$S_c(p) = s_{j,c}, \quad c = 1, \dots, C.$$

Finally, we stack these C similarity maps into a single 3-dimensional array $S \in \mathbb{R}^{H \times W \times C}$ and generate the segmentation mask \hat{Y} by taking a pixel-wise argmax over the class dimension:

$$\hat{Y} = \arg \max (S) \quad (4)$$

3 Experiments and results

3.1 Datasets

We evaluated the ZEUS approach on two in-house WSI collections from distinct hospitals. AI4SkIN [13] includes 90 benign leiomyoma slides from Hospital Clínico Universitario de Valencia (HCUV, 26 WSIs) and Hospital Universitario San Cecilio (HUSC, 64 WSIs). ASSIST comprises 40 secondary cutaneous metastasis WSIs, all from HCUV.

3.2 Experimental settings

We evaluated two state-of-the-art histopathology VLMs—CONCH [11] and KEEP [12]—for this task. Both models use a ViT-based vision encoder and a BERT-style text encoder, pre-trained on large image-text pairs. We first pre-processed the WSIs using CLAM [14] to (1) perform tissue segmentation, (2) partition each slide into 448×448 -pixel patches at an effective magnification of $10\times$ with 75% overlap, and (3) extract feature embeddings for each patch with both models. To compute cosine similarities between image features and text embeddings (Eq. 3), we then design two separate prompt ensembles tailored to the CSC and CM identification tasks each comprising two class prototypes (“tumor” vs. “normal tissue”). Each ensemble consists of multiple textual templates describing the respective WSI types; we use the same number of prompts for both ensembles to ensure comparability across datasets. For evaluation of ZEUS, we report the Dice similarity coefficient (DSC) as in [15], precision, and recall on both AI4SkIN and ASSIST, using pathologist-provided pixel-level annotations from HCUV and HUSC. DSC is defined as:

$$\text{DSC} = \frac{2|\hat{Y} \cap Y|}{|\hat{Y}| + |Y|} \quad (5)$$

where \hat{Y} denotes the predicted binary mask—as defined in Eq. 4—and Y the ground-truth binary mask, with mask values of 1 indicating positive (tumor) pixels.

3.3 Experimental results

Table 1 summarizes the zero-shot segmentation results. On AI4SkIN, CONCH achieves a mean DSC of 84.5%, while KEEP scores 82.9%. Although KEEP’s DSC is marginally lower, it attains higher recall at the expense of a slightly drop in precision. This suggests that KEEP has a higher tendency to over-segment, whereas CONCH is more conservative, balancing precision and recall more evenly. In the more challenging ASSIST dataset of cutaneous metastases, the model gap widens: CONCH’s DSC falls to 57.1%, whereas KEEP reaches 69.5%. KEEP also outperforms CONCH by 5.3% in precision and by 18.7% in recall, with lower variability. These gains underline KEEP’s superior zero-shot handling of heterogeneous secondary tumors.

Dataset	Model	DSC	Precision	Recall
AI4SkIN	CONCH [11]	0.845 ± 0.230	0.822 ± 0.232	0.922 ± 0.200
	KEEP [12]	0.829 ± 0.223	0.767 ± 0.251	0.961 ± 0.160
ASSIST	CONCH	0.571 ± 0.303	0.731 ± 0.217	0.584 ± 0.372
	KEEP	0.695 ± 0.322	0.784 ± 0.201	0.771 ± 0.369

Table 1. Zero-shot segmentation results by model. Results denote the average and standard deviation through all the available WSIs.

These foundational models are mostly pre-trained on large cohorts of primary tumor WSIs, and their embeddings are thus most aligned to the morphological patterns of primary

neoplasms [11, 12]. Our results corroborate this: both CONCH and KEEP achieve high zero-shot DSC on AI4SkIN (primary CSCs). In contrast, on ASSIST (secondary CMs) their performance drops significantly, reflecting the domain shift from primary to metastatic tissue. This differential performance highlights the need for either domain-specific fine-tuning or more diverse pre-training that includes different secondary tumor morphologies to extend foundation models’ zero-shot capabilities beyond primary cancer scenarios.

Prompt design further influences zero-shot performance. For AI4SkIN, we used class-specific descriptors (e.g., “benign tissue,” “leiomyoma”), which align closely with the morphology of primary CSCs and likely contribute to strong DSC performance. By contrast, ASSIST prompt ensembles employ genericclassnames (e.g., “tumor,” “cancerous tissue”) without organ-specific context, since the metastases’ primary site is unknown. This lack of anatomical precision exacerbates the semantic gap for secondary tumors and may underlie the lower DSC on ASSIST.

In addition, in order to investigate institutional biases, we separated AI4SkIN segmentation metrics by source hospital (Table 2). Slides from HUSC consistently outperform those from HCUV by almost 8% on DSC, ratifying prior reports of center-specific domain shifts in digital pathology models [16]. Differences in staining protocols or scanner characteristics can thus materially affect zero-shot segmentation performance. Moreover, inherent variability in pathologist annotations further compounds these discrepancies, as inter-observer differences introduce additional noise into the ground-truth masks. This center-dependent variability highlights the need for center-agnostic pre-training or targeted domain adaptation to ensure reliable deployment of foundation models across diverse clinical settings.

Dataset	Hospital	DSC	Precision	Recall
AI4SkIN	HCUV	0.780 ± 0.167	0.683 ± 0.197	0.968 ± 0.082
	HUSC	0.860 ± 0.241	0.839 ± 0.244	0.931 ± 0.208

Table 2. Center-specific zero-shot segmentation performance on AI4SkIN. Results denote the mean and standard deviation across all WSIs within each center.

3.4 Qualitative analysis

Recent zero-shot segmentation methods often rely on interactive guidance—such as user-selected points or bounding boxes—to delineate tumor regions in histopathology images [9, 10]. While effective, these approaches still demand manual input and cannot be fully automated. By contrast, our framework uses only textual prompts to drive zero-shot segmentation without any further human intervention. In Figure 2, we show a representative AI4SkIN WSI crop overlaid with automatically generated masks from both models alongside the ground-truth annotation. The segmentation closely follows the pathologist’s contour of the leiomyoma, illustrating that zero-shot configurations for VLMs can localize RoIs. Despite these competitive results, our method inherits the

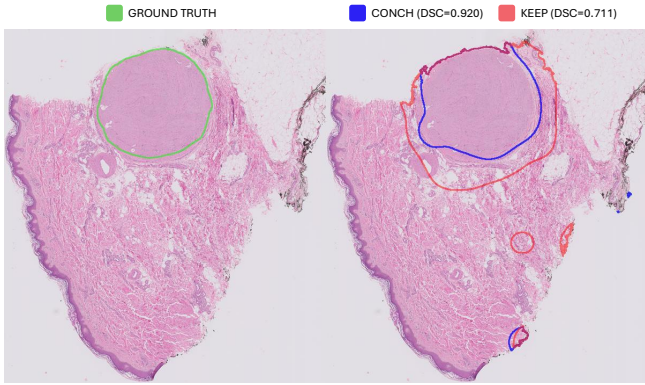


Figure 2. Contours of the predicted segmentation masks for both models CONCH (blue) and KEEP (red) with their respective DSC value, and pathologist annotation (green) on a HUSC leiomyoma WSI.

limitations of patch-level processing. Since each 448×448 patch is far larger than a single pixel, the resulting lesion contours exhibit block-like artifacts and may not capture fine boundary details, which is reflected in the results obtained from smaller dimension tumors and those with irregular shapes. To mitigate this, we applied a 75% patch overlap during WSI partitioning as described in Section 3.2, which effectively creates 'virtual' sub-patches along patch edges and results in smoother and more accurate contours without changing the overall patch size.

4 Conclusion

In this paper, we explored zero-shot segmentation in digital pathology by leveraging VLMs capabilities. We have demonstrated that carefully curated textual prompt sets can be effective semantic anchors for automated identification of complex ROIs. ZEUS pipeline runs completely at inference time, partitioning gigapixel whole-slide images into manageable patches, extracting high-level features, and matching against class ensembles via cosine similarity. Through quantitative and qualitative analysis, we observed that performance varies according to dataset characteristics, primary tumors benefit from precise tissue-specific prompts, while heterogeneous metastases challenge straightforward zero-shot approaches. We also observed how institutional biases, including variability in staining and scanner differences, affect consistency in segmentation between medical centers. Looking ahead, integrating multi-scale context, refining boundary representations, and incorporating domain-adaptive paradigms will be key steps toward robust and generalizable segmentation tools.

References

[1] A. H. Roky, M. M. Islam, A. M. F. Ahasan, M. S. Mostaq, M. Z. Mahmud, M. N. Amin, and M. A. Mahmud, "Overview of skin cancer types and prevalence rates across continents," *Cancer Pathogenesis and Therapy*, vol. 3, pp. 89–100, 3 2025.

[2] J. H. Choi and J. Y. Ro, "Cutaneous spindle cell neoplasms: Pattern-based diagnostic approach," *Archives of Pathology & Laboratory Medicine*, vol. 142, pp. 958–972, 8 2018.

[3] N. Leonard, "Cutaneous metastases: Where do they come from and what can they mimic?," *Current Diagnostic Pathology*, vol. 13, pp. 320–330, 8 2007.

[4] S. K. Danisetty, A. Graikos, S. Yellapragada, and D. Samaras, "Pathsegdiff: Pathology segmentation using diffusion model representations," 2025.

[5] R. del Amor, A. Colomer, S. Morales, C. Pulgarín-Ospina, L. Terradez, J. Aneiros-Fernandez, and V. Naranjo, "A self-contrastive learning framework for skin cancer detection using histological images," *Proceedings - International Conference on Image Processing, ICIP*, pp. 2291–2295, 2022.

[6] M. Bilal, Aadam, M. Raza, Y. Altherwy, A. Alsuhaiabi, A. Abduljabbar, F. Almarshad, P. Golding, and N. Rajpoot, "Foundation models in computational pathology: A review of challenges, opportunities, and impact," 2 2025.

[7] V. Sharma, A. Alagha, A. Khellaf, V. Q.-H. Trinh, and M. S. Hosseini, "Investigating zero-shot diagnostic pathology in vision-language models with efficient prompt design," 4 2025.

[8] I. Ranjbar, Y. Ventikos, and M. Arashpour, "Zero-shot and few-shot multimodal plastic waste classification with vision-language models," *Waste Management*, vol. 202, p. 114815, 7 2025.

[9] H. Liu, H. Yang, P. J. van Diest, J. P. W. Pluim, and M. Veta, "Wsi-sam: Multi-resolution segment anything model (sam) for histopathology whole-slide images," 3 2024.

[10] C. Cui, R. Deng, J. Guo, Q. Liu, T. Yao, H. Yang, and Y. Huo, "Pfps: Prompt-guided flexible pathological segmentation for diverse potential outcomes using large vision and language models," 7 2024.

[11] M. Y. Lu, B. Chen, D. F. Williamson, R. J. Chen, I. Liang, T. Ding, G. Jaume, I. Odintsov, L. P. Le, G. Gerber, A. V. Parwani, A. Zhang, and F. Mahmood, "A visual-language foundation model for computational pathology," *Nature Medicine*, vol. 30, pp. 863–874, 3 2024.

[12] X. Zhou, L. Sun, D. He, W. Guan, R. Wang, L. Wang, X. Sun, K. Sun, Y. Zhang, Y. Wang, and W. Xie, "A knowledge-enhanced pathology vision-language foundation model for cancer diagnosis," 12 2024.

[13] R. del Amor, M. López-Pérez, P. Meseguer, S. Morales, L. Terradez, J. Aneiros-Fernandez, J. Mateos, R. Molina, and V. Naranjo, "A fusocellular skin dataset with whole slide images for deep learning models," *Scientific Data*, vol. 12, pp. 1–7, 12 2025.

[14] M. Y. Lu, D. F. Williamson, T. Y. Chen, R. J. Chen, M. Barbieri, and F. Mahmood, "Data-efficient and weakly supervised computational pathology on whole-slide images," *Nature Biomedical Engineering*, vol. 5, pp. 555–570, 6 2021.

[15] J. Silva-Rodríguez, J. Dolz, and I. B. Ayed, "Towards foundation models and few-shot parameter-efficient fine-tuning for volumetric organ segmentation," *Lecture Notes in Computer Science (including subseries Lecture Notes in Artificial Intelligence and Lecture Notes in Bioinformatics)*, vol. 14393, pp. 213–224, 2023.

[16] E. D. de Jong, E. Marcus, and J. Teuwen, "Current pathology foundation models are unrobust to medical center differences," 1 2025.